Estuarine, Coastal and Shelf Science 164 (2015) 433–442

Contents lists available at ScienceDirect

Estuarine, Coastal and Shelf Science

journal homepage: www.elsevier.com/locate/ecss

Mapping estuarine habitats using airborne hyperspectral imagery, with special focus on seagrass meadows

Mireia Valle [a, b, *], Vicenç Palà [c], Virgine Lafon [d], Aurélie Dehouck [d], Joxe Mikel Garmendia [e], Ángel Borja [e], Guillem Chust [a]

[a] AZTI, Marine Research Division, Txatxarramendi ugartea z/g, 48395, Sukarrieta, Spain
[b] Universidad Laica Eloy Alfaro de Manabí, Central Research Department, Ciudadela Universitaria, vía San Mateo s/n, 13-05-2732, Manta, Ecuador
[c] Institut Cartogràfic i Geològic de Catalunya, Catalan Earth Observation Program, Parc de Montjuïc, 08038, Barcelona, Spain
[d] GEO Transfert, UMR EPOC, CNRS – Université de Bordeaux, Avenue des Facultés, 33405, Talence Cedex, France
[e] AZTI, Marine Research Division, Herrera Kaia Portualdea z/g, 20110, Pasaia, Spain

ARTICLE INFO

Article history:
Received 25 November 2014
Received in revised form
13 May 2015
Accepted 26 July 2015
Available online 5 August 2015

Keywords:
Habitat classification
Estuaries
Remote sensing
Zostera noltii
Compact airborne spectrographic imager

ABSTRACT

Estuaries and coasts are among the most productive ecosystems and constitute valuable habitats for biodiversity and ecosystem services. Amongst nearshore ecosystems, seagrass beds play a major role enhancing biodiversity and water quality. Consequently, the development of new approaches to create extensive and high-resolution habitat maps is required not only to implement conservation, restoration and management plans, but also to establish adaptation plans to face climate change impacts. This study particularly assesses the capability of hyperspectral airborne imagery acquired with Compact Airborne Spectrographic Imager (CASI) to discriminate and map estuarine habitats, with special focus on *Zostera noltii* seagrass meadows. To this end, 13 habitats were defined along the supralittoral, intertidal and subtidal zones of an estuary, including *Z. noltii* seagrass meadows. The CASI sensor was configured to acquire 25 bands in the visible and near infrared wavelengths with a ground sampling distance of 2 m. Spectral bands were selected for species discrimination based on the spectral signature of the different habitat classes. Six different band combinations were tested applying maximum likelihood classification algorithm. The most accurate classification was obtained with 10 band combination (a mean producer accuracy 92% and a mean user accuracy 94%). The classification of *Z. noltii* beds has been found to be restricted to moderate and high dense meadows, however a vegetation index has been defined which could be applied for mapping *Z. noltii* meadow cover. These results highlight the value of CASI data to discriminate and map estuarine habitats, providing key information to be used in supporting the implementation of environmental legislation, protection and conservation of coastal habitats.

1. Introduction

Estuaries and coasts are among the most productive ecosystems and constitute valuable habitats for biodiversity (Barbier et al., 2011) and ecosystem services (Costanza et al., 1997, 2014). Amongst nearshore ecosystems, seagrass beds play a major role enhancing biodiversity and water quality (Duarte, 2002; Green and Short, 2003; Beamount et al., 2007) and, accordingly, these plants are regarded as a useful indicators due to their sensitivity to anthropogenic pressures, being highly relevant as one of the biological quality elements required for the assessment of the ecological quality status in coastal and transitional water bodies within the European Water Framework Directive (WFD, 2000/60/EC). However, the estuarine and coastal habitats have been historically altered and degraded (Halpern et al., 2008; Lotze, 2010) and seagrass beds in particular, are undergoing a global decline (Waycott et al., 2009). Moreover, in the coming decades, coastal systems and low-lying areas will increasingly experience adverse climate-related impacts (IPCC, 2014) exacerbated by increasing human-induced pressures (Wong et al., 2014). Concern about the negative repercussions derived from the loss of biodiversity and ecosystem functions of these habitats has triggered the development of conservation frameworks worldwide (Worm et al., 2006). In order to assess the ecosystem status and the influence of natural

* Corresponding author. Current address: Universidad Laica Eloy Alfaro de Manabí, Central Research Department, Ciudadela Universitaria, vía San Mateo s/n, 13-05-2732, Manta, Ecuador.
E-mail address: mireia.valle@uleam.edu.ec (M. Valle).

http://dx.doi.org/10.1016/j.ecss.2015.07.034
0272-7714/

and anthropogenic impacts over time, development of new approaches to create extensive and high-resolution habitat maps is required (Chust et al., 2010). Such spatial information is of major importance not only to implement conservation, restoration and management plans of natural resources, but also to establish adaptation plans to face climate change impacts (Hoepffner, 2006).

Mapping terrestrial or shallow biodiversity by traditional on-ground sampling methods has become non cost-effective in the face of remote sensing techniques, mainly due to: (i) sampling-point field work is not adequate for covering extensive areas in high detail; (ii) mapping large areas cannot be accomplished in a reasonable time (Dekker et al., 2006), and (iii) several habitats are inaccessible. In contrast, spaceborne and airborne optical remote sensing have the potential to quickly and cost-efficiently map large terrestrial and shallow areas with high resolution (Herkül et al., 2013). In addition, remote sensing data can also be used to perform time-series analysis in order to understand temporal and spatial dynamics of different habitats (Lyons et al., 2013). A further advantage of acquiring remote sensing data is that the products can be analysed with different purposes over time. According to Phinn et al. (2008), airborne image data can achieve more accurate results than satellite multispectral data, mainly due to the high spatial resolution of the data (which allows for a better delineation of small or patchy habitats) and the high radiometric resolution (which increases the level of mapping precision). The use of airborne instead of spaceborne imagery also benefits from a user-programmable date of acquisition at optimal tidal and weather conditions (Finkbeiner et al., 2001) and programmable limits of the spectral bands (Chen et al., 1999). These are two important factors to consider since estuarine habitats are subjected to tidal submergence and selection of the spectral bands could enhance the vegetation differentiation. Airborne hyperspectral imagery was selected for the present study as it provides high spectral, spatial, and radiometric resolution with high signal-to-noise ratio (Dekker et al., 2006). Data were acquired with a CASI sensor, which is a push-broom imager capable of configurable image collection in visible and near-infrared wavelength regions (i.e. limits of the spectral bands are programmable) (Chen et al., 1999). Airborne hyperspectral imagery has been found to produce the highest overall accuracies in comparison to satellite multispectral at high and moderate spatial resolution (Phinn et al., 2008). Airborne remote sensing has been also found to overcome the spatial limitations inherent in conventional satellite sensors for accurate monitoring of small-scale dynamics (Dekker et al., 2006). Furthermore, hyperspectral airborne sensor data provide significantly more biological information than conventional spaceborne sensors and is a geometrically accurate, cost-effective alternative to aerial photography (Mumby et al., 1997).

Although presenting such a wide range of advantages, more investigation is still needed to evaluate the discrimination potential of several estuarine vegetation species (such as *Z. noltii*) either from space sensors or airborne hyperspectral imagery (Dehouck et al., 2012). Thus, this research aims to assess the capability of hyperspectral airborne imagery acquired with compact airborne spectrographic imager (CASI) to discriminate and map estuarine habitats, with special focus on *Z. noltii* seagrass meadows. This contribution will also provide a baseline mapping for monitoring the wetland, saltmarshes and mudflats communities of the region and the methods presented might be applied to other estuaries where *Z. noltii* meadows occur.

2. Material and methods

2.1. Study area

The selected study area (Oka estuary, Basque Country, Spain, Fig. 1) covers an area of 10.27 km^2, being 86% intertidal area (Borja et al., 2006) and encompassing the environmental conditions of those estuaries from the Bay of Biscay coast (northern Spain and southern France) which are classified as 'estuaries with extensive intertidal flats' within the WFD (2000/60/EC). The large intertidal flats of this estuary are characterised by *Z. noltii* seagrass meadows (Valle et al., 2011) and associated macroalgae (*Ulva* sp. and *Gracilaria* sp.). Particularly on the Basque coast (Fig. 1), *Z. noltii* is the only occurring seagrass species and has been recently listed as an endangered species within the Catalogue of Threatened Species in the Basque Country (BOPV, 2011). Its best preserved and largest *Z. noltii* meadows are located in this estuary, hosting up to 86.9% of total seagrass coverage in the region (Garmendia et al., 2013). The upper tidal levels of the Oka estuary are occupied by coastal saltmarshes formed by halophytic plant communities (Chust et al., 2010). These intertidal mud and sand flats constitute valuable habitats regarding to biodiversity and ecosystem functioning, since they are critical breeding and nesting habitats for birds and fish, they act as water filtering systems and they enhance the stability of estuarine substrata (Rönnbäck et al., 2007).

This estuary is one of the most biologically diverse and best conserved of the region, together with the Bidasoa estuary (Borja et al., 2004) (Fig. 1). Therefore, it is included under a wide range of national and international protection and conservation frameworks; and, consequently, it has been investigated extensively (Castro et al., 2004). Chust et al. (2010) performed an assessment of the classification of 22 habitats along the subtidal, intertidal and supralittoral zone of this estuary using Light Detection And Ranging (LiDAR) topographic and bathymetric data acquired in 2008. Due to the high morphodynamism inherent in estuarine habitats between the date of acquisition for the LiDAR data (i.e. in 2008) and CASI (i.e. in 2012), especially in sandy areas in the upper estuary, the digital elevation model was included in the present study.

2.2. Remote sensing data

The CASI sensor was configured to acquire 25 selected bands characterised by the same spectral width (Table 1) at 2 m GSD (Ground Sampling Distance). Selection of the spectral bands was adjusted for species discrimination based on the spectral signature of *Z. noltii* meadows, associated macroalgae and coastal saltmarshes (Fyfe, 2003; Dekker et al., 2005; Costa et al., 2007; Thorhaug et al., 2007; Jollineau and Howarth, 2008; Phinn et al., 2008). This selection is likely to optimize the vegetation differentiation (Dekker et al., 2006).

Airborne imagery was collected on July 3rd, 2012 under clear sky conditions and the lowest tide level (1.05 m), using the hyperspectral imager CASI 550 property of the Institut Cartogràfic i Geològic de Catalunya (ICGC). The flight was planned in early summer for climatological reasons and also to benefit of well-developed intertidal plant and macroalgae canopies. The imagery was acquired in the solar plane in order to minimize the sunlight intrusion, at a velocity of 121 knots and an altitude of 1495 m, so the 40.4° CASI field of view resulted in a nominal swath width of 1.1 km (2 m by 550 pixels). The aircraft flew 22 individual flight lines which were mosaicked by a feathering technique of 2 pixels (weighted mean of overlapped pixels).

The image processing included radiometric (Babey and Soffe, 1992), geometric (Colomina et al., 1995; Alamús et al., 1999) and atmospheric (Martínez et al., 2006) corrections. The overall geometric accuracy assessment of the acquired imagery was performed by the ICGC, obtaining an RMSE (Root Mean Square Error) smaller than the GSD (Light, 1986). However, with the aim to detect bands with high radiometric differences from one individual scene

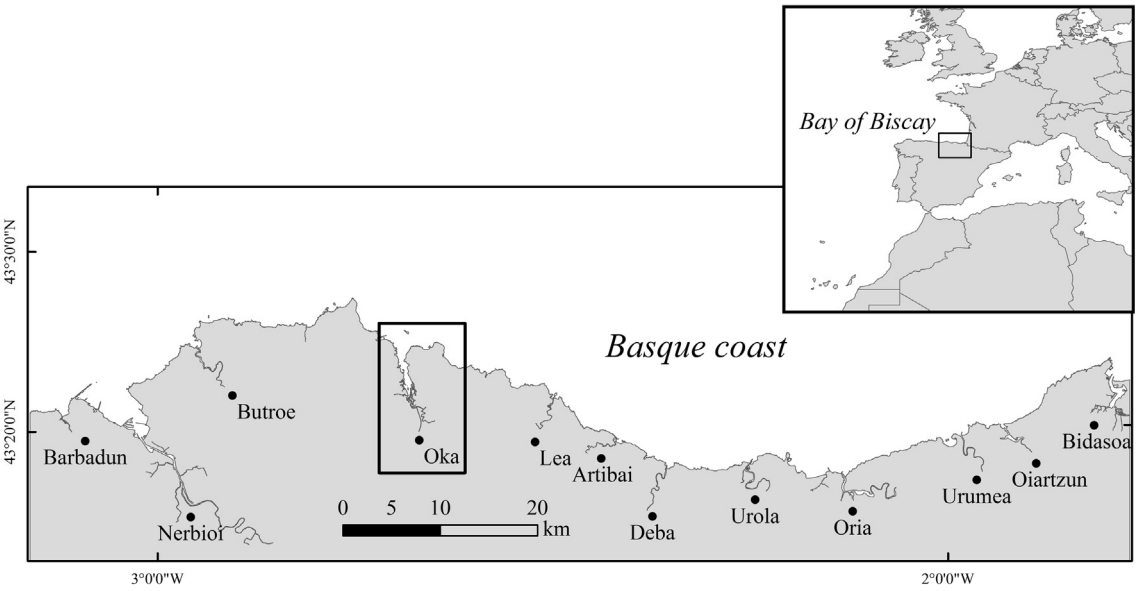

Fig. 1. The Basque coast within the SE Bay of Biscay. Map showing the 12 main estuarine ecosystems of the coast. Oka estuary (43° 22′ N, 2° 40′ W) highlighted within a rectangle.

Table 1
Preprogrammed band set configuration of Compact Airborne Spectrographic Imager (CASI) sensor for data acquisition.

Band	Centre (nm)	Width (nm)	Start (nm)	End (nm)	Description
1	411.54	9.46	416.27	406.81	Blue
2	432.33	9.44	437.05	427.61	Blue
3	488.88	9.41	493.59	484.18	Blue
4	511.47	9.41	516.17	506.76	Green
5	535.92	9.41	540.62	531.22	Green
6	550.97	9.41	555.67	546.27	Green peak
7	560.38	9.41	565.08	555.67	Green
8	571.67	9.41	576.37	566.96	Green
9	582.96	9.41	587.67	578.25	Yellow
10	596.14	9.42	600.85	591.43	Orange
11	614.99	9.43	619.71	610.28	Orange
12	630.08	9.44	634.8	625.37	Red
13	645.19	9.45	649.92	640.47	Red
14	667.89	9.47	672.63	663.16	Red
15	679.26	9.48	684	674.52	Red
16	694.45	9.5	699.19	689.7	Red edge
17	705.85	9.51	710.6	701.09	Red edge
18	719.17	9.53	723.94	714.41	Red edge
19	736.34	9.55	741.12	731.57	Red edge
20	747.81	9.57	752.6	743.03	Red edge
21	784.27	9.63	789.09	779.46	Near-infrared
22	811.29	9.67	816.13	806.46	Near-infrared
23	857.96	9.77	862.84	853.07	Near-infrared
24	899.19	9.87	904.12	894.26	Near-infrared
25	948.83	9.99	953.83	943.84	Near-infrared

(corresponding to a flight-line) to another, composites of 3 bands were visualised after image correction. These radiometric differences between neighboring images are related to the different observation angles of the overlapping areas and the non-lambertian properties of the covers, especially the water, causing artifacts in the final mosaic, more accentuated for some specific bands.

2.3. Field measurements

2.3.1. Regions of interest

Ground-truth sampling was carried out concurrently with the remote sensing campaign to provide field reference data for image classification. In addition to this specific sampling, data from a ground survey conducted by Chust et al. (2010) were also considered for image classification training and validation. The sampling consisted of delimiting several areas (regions of interest, ROIs hereafter) for each defined habitat class along supralittoral, intertidal and subtidal zones (Table 2 and Figs. A.1 and A.2).

The ROIs were as homogenous as possible according to substratum type, vegetation cover, macroalgae and plant species. Covered areas consisted in 6 × 6 m polygons for all habitat classes except for *Z. noltii* habitat classes which covered an area of 4 × 4 m due to the patchy composition of the meadows of this species. The location of each ROI (114 within intertidal habitats and 32 within *Z. noltii* meadows) was determined with a high precision GPS deliver Trimble R6 GNSS system (maximum horizontal position error of 1.5 cm and maximum vertical position error of 2 cm). Digital photographs of each ROI were captured from a 4 m height pole during the sampling (Figs. A.1 and A.2). Ground-truth data were randomly divided into two independent data sets (Table 2), one to calculate the statistics needed for the classification (i.e. training sites) and the other to evaluate the reliability of the classifications (i.e. validation sites).

2.3.2. Seagrass meadows: cover and spectral signature

Simultaneously to the ground-truth sampling, data on *Z. noltii* shoot density were also acquired along a percent cover gradient (0–25%; 25–50%; 50–75%; 75–100%) in order to obtain detailed data on *Z. noltii* spectral response and enable the application of a Normalized Difference Vegetation Index ($NDVI_z$ see below). Thus, the ROIs corresponding to *Z. noltii* habitat class included the information on the patch cover and on the shoot density. Shoot density was sampled deploying a 25 × 25 cm frame in the middle part of the ROI (where the location was acquired) and counting the number of shoots within the frame. Digital photographs of each sample point were captured from 1 m height.

Based on the photographs we compared the percent cover estimated by *visu* (i.e. the percent of substratum covered by *Z. noltii* when viewed directly from above) to that estimated by a supervised classification performed in ENVI image analysis software (ENVI 4.2) using the maximum likelihood method (ML, explained further in this subsection). Photographs covered an area of 50 × 50 cm. The percent cover estimates derived from the ML

Table 2
Description of the classes defined for habitat classification (see also Figs. A.1 and A.2). ROIs: Regions of interest.

	Description	Training ROIS	Validation ROIs
Vegetated dunes	Embrionary, secondary, tertiary and artificial dunes with fine sand dominated by psammophilic vegetation such as *Ammophila arenaria (subsp. australis)*, *Euphorbia paralias*, *Elymus farctus (susp. boreali-atlanticus)* and *Calystegia soldanella*.	2931 pixels 10.55 ha	1354 pixels 4.87 ha
Phragmites australis	High vegetation zone (upper saltmarsh) which suffers weak tidal influence, flooded only during high spring tides. Practically mono-specific formation dominated by *Phragmites australis*.	96 pixels 0.35 ha	92 pixels 0.33 ha
Saltmarshes	Placed in the inner part of the estuary of low hydrodynamism. Middle vegetation zone (low-intermediate saltmarsh), flooded twice a day, and dominated by vascular halophilic plants such as *Juncus maritimus*, *Halimione portulacoides*, *Sarcocornia fruticosa*, *Sarcocornia perennis*, *Salicornia dolichostachya*, *Salicornia lutescens*.	327 pixels 1.18 ha	345 pixels 1.24 ha
Green macroalgae	Low and mid intertidal muddy shore in the middle and upper part of the estuary dominated by the macroalgae *Ulva clathrata* and *Ulva rigida*.	81 pixels 0.29 ha	80 pixels 0.29 ha
Gracilaria sp. with *Ulva* sp.	Low and mid intertidal muddy shore in the middle and upper part of the estuary dominated by the macroalgae *Gracilaria* sp. mixed with *Ulva rigida* and *Ulva compressa*. With small patches of *Chaetomorpha linum* and *Chaetomorpha ligustica*.	48 pixels 0.17 ha	48 pixels 0.17 ha
Vegetated mudflats	Low and mid intertidal muddy shore in the middle and upper part of the estuary partially vegetated by macroalgae (*Vaucheria* spp.) and microalgae.	64 pixels 0.23 ha	48 pixels 0.17 ha
Zostera noltii 20%–55%	Low dense (20%–55% of surface cover) marine seagrass beds of *Z. noltii* on sandy and muddy substrates at intertidal zone.	31 pixels 0.05 ha	25 pixels 0.04 ha
Zostera noltii > 55%	High dense (larger than 55% of surface cover) marine seagrass beds of *Z. noltii* on sandy and muddy substrates at intertidal zone.	26 pixels 0.04 ha	27 pixels 0.04 ha
Infralitoral sand flats	Sand shores placed in the mid-low estuary exclusively constituted by fine sand, subjected to tidal submergence.	6212 pixels 22.36 ha	41 pixels 0.15 ha
Supralitoral sand flats	Sand shores placed in the upper estuary exclusively constituted by fine sand and shell fragments.	4708 pixels 16.95 ha	500 pixels 1.80 ha
Water mass	Water channels and sea water.	2634 pixels 9.48 ha	2611 pixels 9.40 ha
Mudflats	Fine sediment (sandy mud) with low organic matter content. Low and mid intertidal muddy shore in the middle and upper part of the estuary, subjected to tidal submergence.	146 pixels 0.53 ha	66 pixels 0.24 ha
Riparian woodland	Riparian woodland associated to rivers placed around wetlands in soils rich in alluvial deposits. Dominance of *Alnus glutinosa*, *Tamarix gallica*, *Fraxinus excelsior* and *Salix* sp.	1329 pixels 4.78 ha	944 pixels 3.40 ha
Pastures	Traditionally drained areas to be used for agricultural purposes and pasture land.	7144 pixels 25.72 ha	3681 pixels 13.25 ha

classification were used to define the habitat class of *Z. noltii* to which each sampled ROI belong to (i.e. low dense or high dense).

2.3.3. Spectral signatures

In addition to the field sampling carried out the same day of the flight, *in situ* reflectance measurements of the different estuarine habitats which were selected for classification (Table 2) were also undertaken one week after the imagery acquisition using TriOS radiance/irradiance field sensors. Measurements were conducted by GEO-Transfert (University of Bordeaux) in the framework of the SYNIHAL project. The radiance of each habitat class was measured at nadir. Reflectance for each habitat was estimated as the ratio of the radiance of the habitat surface, to the incident downwelling irradiance. The spectral reflectance measurements were analysed in order to identify changes in the spectrum between the habitat classes and were compared to that spectrum extracted from the imagery in the ROIs.

2.4. Normalized difference vegetation index for Z. noltii

Spectral responses of *Z. noltii* at different percent covers were extracted from the CASI imagery in the sampled ROIs. In order to relate the spectral response of *Z. noltii* to its density and surface cover, a Normalized Difference Vegetation Index (NDVI) was calculated combining the reflectance in the red and infrared regions (Rouse et al., 1973; Tucker, 1979). NDVI is the most widely used index to assess green biomass (Lillesand and Kiefer, 2000). The wavelengths selected to calculate the NDVI for *Z. noltii* ($NDVI_z$) were determined based on the changes in the spectral response of *Z. noltii* in reference to the percent cover. A non-linear regression between the $NDVI_z$ and the *Z. noltii* cover was subsequently calculated following Bargain et al. (2012). The data were modeled by the exponential function:

$$NDVI_Z = a + b\left(1 - e^{-c*cover}\right) \quad (1)$$

where a is the intercept, b is the asymptotic value (=$NDVI_{zmax}$) and c the slope value.

2.5. Habitat classification

Final corrected images from the CASI and the ground-truth data were imported into the ENVI image analysis software (ENVI 4.2) to perform the image classification using a supervised classification approach. Supervised classification was considered to be the most appropriate approach versus non-supervised approaches, since the study area was well-known and accessible allowing field sampling for ROIs acquisition (Lillesand and Kiefer, 2000). Amongst the different supervised classification approaches, the widely used ML supervised classification approach method was selected (Jensen, 2007). This method computes the probability of each pixel to belong to one of the predefined habitat classes and assigns it to the class to which it most likely belongs. ML algorithm considers the variability in each ROI and assumes that training data statistics in each band for each class are normally distributed (Peneva et al., 2008).

In order to achieve the best classification, the acquired spectral bands were combined in different groups and their accuracy was assessed. Firstly, a classification was computed by introducing all acquired spectral bands except the bands 1 and 2 (excluded in order to minimize artifacts derived from radiometric differences between swaths). This classification based on 23 bands was compared to: (i) a combination of three visible bands (bands 3, 7 and 12) conventionally used for photo-interpretation; (ii) a combination of three visible bands (bands 3, 7 and 12) plus a band in the near-infrared

(band 22); (iii) a combination of six visible bands (bands 3, 7, 14, 15, 18 and 20) plus a band in the near-infrared (band 22); (iv) a combination of nine visible bands (bands 3, 4, 7, 12, 14, 15, 16, 18 and 20) plus a band in the near-infrared (band 22), and (v) a combination of eleven visible bands (bands 4, 5, 7, 8, 13, 14, 15, 17, 18, 19 and 20) plus four bands in the near-infrared (bands 21, 22, 23 and 24). Band combinations were selected based on the differences in the spectral response between habitat classes (Figs. 2 and 3).

The classification accuracy of each combination of bands was assessed on the basis of the accuracy measurements derived from the confusion matrices (Stehman, 1997; Foody, 2002). A confusion matrix represents a cross-tabulation of the mapped class against the ground-truth data (Congalton, 1991). The per class accuracy indices were: (i) the producer accuracy (PA), which indicates the probability of a certain category defined by the reference data to be classified as the same category by the map; and (ii) the user accuracy (UA), which shows the probability of an area classified as a certain category by the map to be defined as the same class by the reference data. The overall accuracy measurements used were: the mean producer accuracy (MPA; i.e. the mean of all PA), the mean user accuracy (MUA; i.e. the mean of all UA), and the Kappa coefficient of agreement (Stehman, 1997). The Kappa coefficient of agreement value ranges from 1 to −1, where 1 means full agreement between habitat classification and validation, −1 indicates full disagreement, and 0 indicates that observed agreement is random. This index accommodates for the effects of chance agreement (Foody, 2002), taking into account that the classes may differ in size. In order to evaluate the capability of the hyperspectral imagery to discriminate and map *Z. noltii* meadows, the most accurate band combination was compared to a recent GPS-based cartography of the same year undertaken by Garmendia et al. (2013).

3. Results

3.1. Spectral signatures

Spectral reflectance curves were analysed for the habitats selected with classification purposes (Fig 2). The spectral response of the habitats within sandy substratum (vegetated dunes and supralittoral sand flats) presented high reflectance in the visible part (from 380 nm to 750 nm) (Fig. 2). This is related to the low water and organic content of the sandy sediment (Bargain et al., 2012). Green plant species had significantly lower reflectance in the visible part of the spectrum due to the absorption by photosynthetic and accessory pigments, especially in the range from 400 to 500 nm and around the 675 nm. The spectrum from green macroalgae and saltmarshes (*Halimione portulacoides* and *Sarcocornia* sp.) showed higher reflectance in the visible part than *Gracilaria* sp. and *Juncus maritimus* (Fig. 2).

The recorded spectrum within *Z. noltii* meadows above muddy sand, showed high reflectance in the visible part and low absorption around 675 nm (Fig. 2), likely related to the background sandy sediment. Deeper absorption in the visible part and sharper rise in the near-infrared was recorded in the sampling points where the cover of *Z. noltii* was total (Fig. 2).

Once the *in situ* measurements of the spectral response were analysed, spectral signatures of each defined habitat class were extracted from the imagery acquired with the CASI using the ROIs (Fig. 3). The extracted spectra allowed identifying the wavelengths for which the habitats can be discriminated. Spectral signatures for the different ROIs along the *Z. noltii* cover gradient were also extracted from the CASI imagery (Fig. 3).

In accordance with the spectra from the *in situ* reflectance measurements (Fig 3) lower radiance was detected in all the

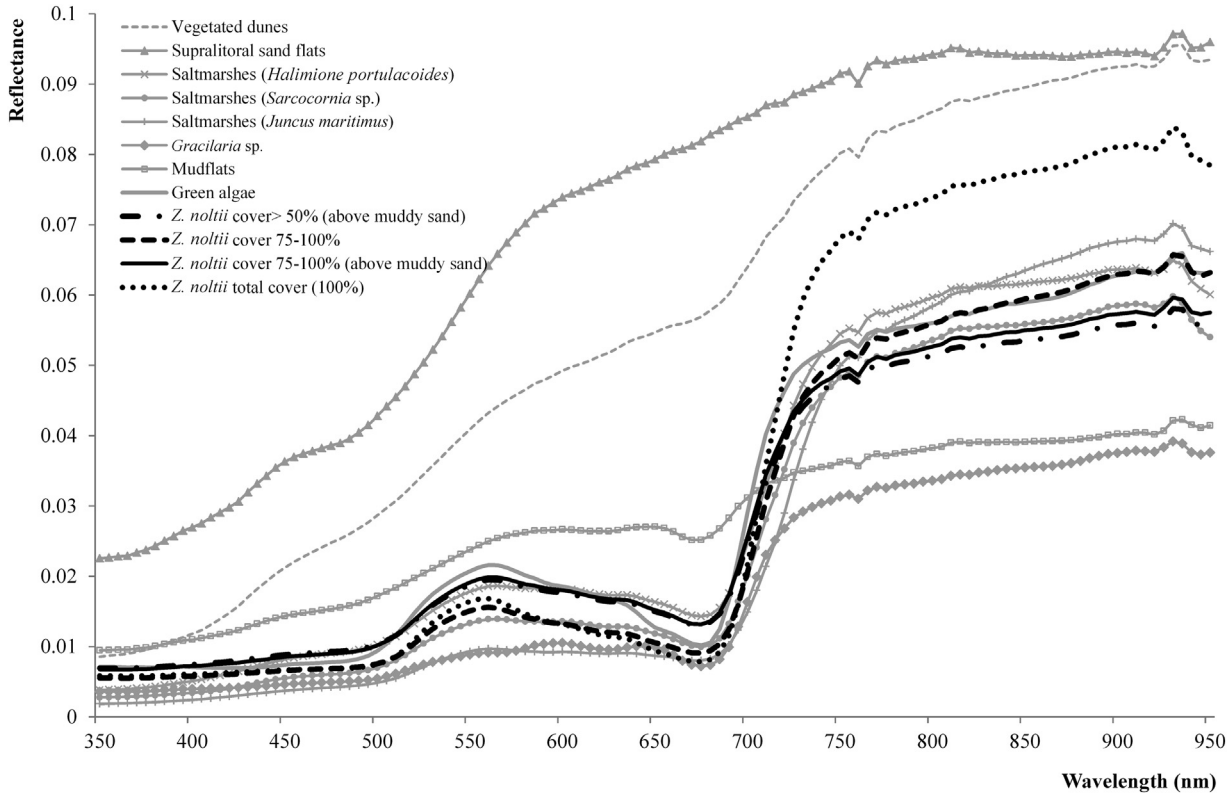

Fig. 2. Reflectance spectra of the habitats within supralittoral and the intertidal zone and of *Zostera noltii* at different covers and background sediment types.

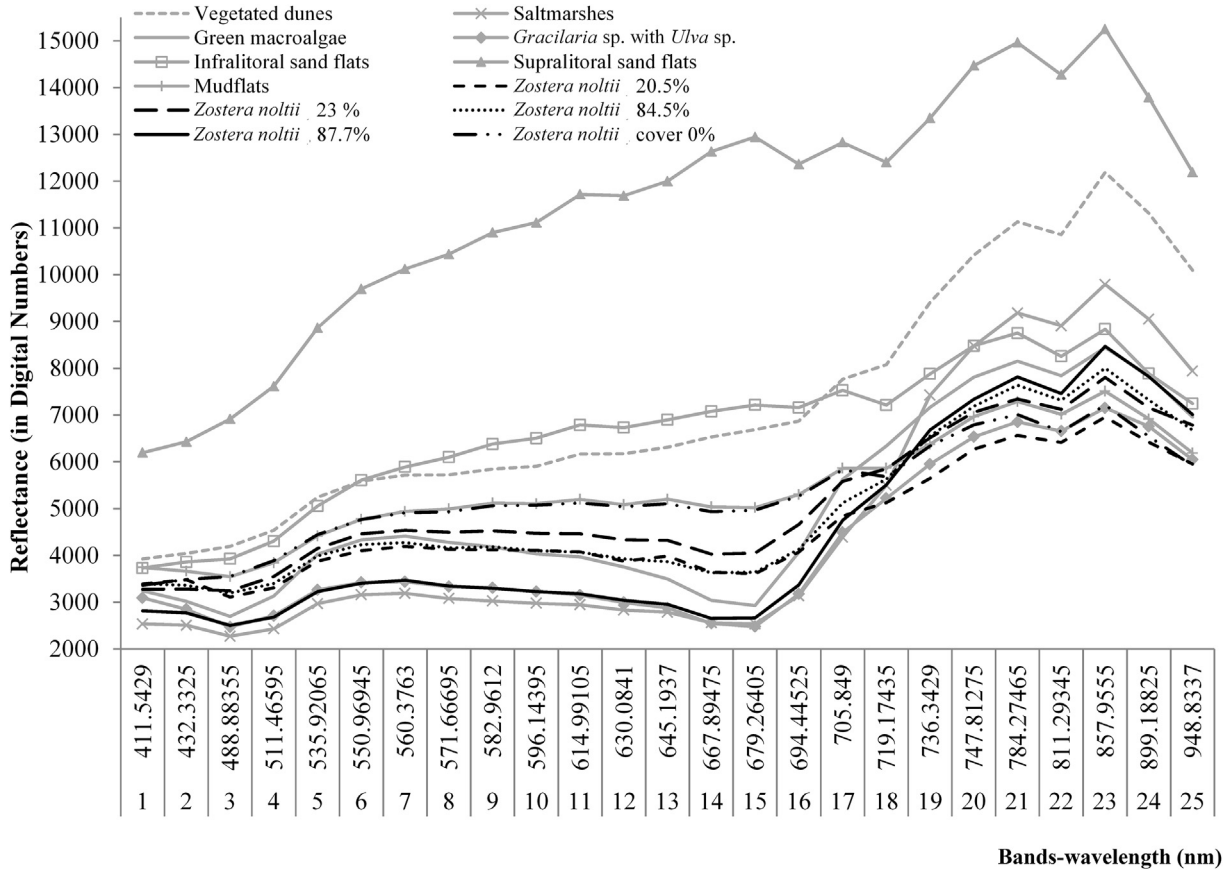

Fig. 3. Spectral signatures of intertidal habitats and for the different Regions Of Interest (ROIs) along the *Zostera noltii* cover gradient (in %) extracted from the Compact Airborne Spectrographic Imager (CASI) imagery using the ground-truth data.

vegetated ROIs than in the unvegetated ones (Fig. 3). Around the 675 nm wavelength, the major absorption values were observed for the ROIs where the percent cover of *Z. noltii* was higher than 84%. Those ROIs with the highest cover showed the highest radiance in the near-infrared.

3.2. Normalized difference vegetation index for Z. noltii

Based on the detected changes in the spectrum, the wavelengths 679.26 nm (band 15, red) and 784.27 nm (band 21, near-infrared) were selected to calculate the $NDVI_z$ index as:

$$NDVI_z = \frac{R_{784.27} - R_{679.26}}{R_{784.27} + R_{679.26}} \quad (2)$$

Subsequently the non-linear regression indicated in eq. (1) was computed (coefficient of determination $R^2 = 0.59$) (Fig. 4). Based on the results from the non-linear model a threshold of percent cover was identified (55%) and two different percent cover ranges were defined to perform the habitat classification: (i) from 20 to 55%; and (ii) higher than 55%.

An $NDVI_z$ lower than 0.25 was detected for bare sediments or sediments with very low cover of *Z. noltii* (below 20%). An $NDVI_z$ value ranging between 0.25 and 0.35 grouped the 85% of the *Z. noltii* ROIs with a cover gradient between 20% and 55%. The 100% of the *Z. noltii* ROIs representing dense meadows (percent cover > 55%) presented an $NDVI_z$ greater than 0.35. The misclassification of 15% of ROIs with a cover gradient between 20% and 55% could be related to the background influence of the sediment, which produces high an $NDVI_z$ value (>0.35).

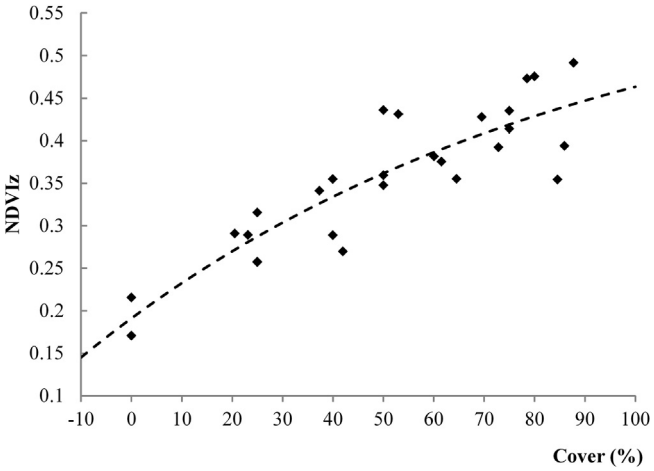

Fig. 4. Non-linear regression model, estimated by exponential function between the Normalized Difference Vegetation Index (NDVIz) and the *Zostera noltii* cover.

3.3. Habitat classification

Comparison on different combinations of bands showed that the classification based on 10 bands presented the highest classification accuracy for the 14 habitats selected along the subtidal, intertidal and supralittoral zone (Table 3). This classification provided the highest mean producer and user accuracy and the best kappa value (Table 3). However, overall accuracy of all tested classification was

Table 3
Accuracy assessment results for each band combination. Overall accuracy measures: Kappa; mean producer accuracy (MPA); mean user accuracy (MUA). Results per habitat class for each band combination (in %). PA: producer accuracy, MPA per class indicates the mean producer accuracy achieved by each class based on the tested classification. UA: user accuracy, MUA per class indicates the mean user accuracy achieved by each class based on the tested classification.

	3 bands		4 bands		7 bands		10 bands		15 bands		23 bands		Mean accuracy per class (%)	
Kappa	0.8698		0.9808		0.9862		0.9886		0.9874		0.9838			
MPA	82.58		91.59		91.39		91.88		87.53		80.68			
MUA	67.09		91.16		92.36		93.26		92.9		93.75			
Class	PA	UA	PA	UA	PA	UA	PA	UA	PA	UA	PA	UA	MPA	MUA
Vegetated dunes	97.12	96.98	99.85	99.93	99.85	99.85	99.70	99.85	99.70	99.85	99.41	99.85	99.27	99.39
Phragmites australis	82.61	16.56	88.04	87.10	85.87	95.18	89.13	90.11	80.43	94.87	69.57	98.46	82.61	80.38
Saltmarshes	92.71	83.91	95.92	88.44	96.21	91.92	96.79	94.05	97.67	95.44	99.13	88.08	96.41	90.31
Green macroalgae	88.75	22.83	95.00	98.70	92.50	96.10	95.00	97.44	100.00	89.89	98.75	86.81	95.00	81.96
Gracilaria sp. with *Ulva* sp.	35.42	19.77	91.67	88.00	81.25	90.70	81.25	92.86	79.17	84.44	56.25	90.00	70.84	77.63
Mudflats	96.97	69.57	98.48	94.20	100.00	95.65	100.00	97.06	100.00	97.06	100.00	91.67	99.24	90.87
Vegetated mudflats	95.83	83.64	97.92	95.92	95.83	95.83	97.92	95.92	87.50	100.00	79.17	100.00	92.36	95.22
Zostera noltii 20%–55%	60.00	33.33	68.00	60.71	76.00	59.38	72.00	62.07	52.00	54.17	20.00	62.50	58.00	55.36
Zostera noltii > 55%	44.44	22.22	55.56	68.18	55.56	71.43	55.56	78.95	29.63	88.89	7.41	100.00	41.36	71.61
Supralitoral sand flats	97.40	96.82	100.00	99.80	100.00	99.60	100.00	99.21	100.00	99.21	100.00	98.43	99.57	98.85
Water mass	87.44	98.36	100.00	99.69	100.00	99.66	100.00	99.66	100.00	99.69	100.00	99.62	97.91	99.45
Infralitoral sand flats	92.68	100.00	95.12	100.00	97.56	100.00	100.00	100.00	100.00	100.00	100.00	100.00	97.56	100.00
Riparian woodland	98.20	95.47	98.62	95.68	99.79	97.82	99.58	98.53	99.68	97.21	99.89	97.22	99.29	96.99
Pastures	86.53	99.84	98.04	99.83	98.99	99.86	99.38	99.95	99.62	99.92	99.89	99.92	97.08	99.89

very high (kappa value > 0.98) except for the classification based on the three bands from the visible spectrum (kappa value = 0.86) (Table 3).

Regarding the obtained accuracy values per class (or habitat type), the best classification results were obtained for vegetated dunes, vegetated mudflats, supralittoral sand and riparian woodland (Table 3). The two *Z. noltii* classes presented high confusion (i.e. misclassification) in comparison to the rest of habitat classes (Table 3). The classification based on the 23 bands was found to be the worst: not only *Z. noltii* classes resulted in being misclassified but also *Phragmites australis*, *Gracilaria* sp. with *Ulva* sp., and vegetated mudflats (Table 3). In the remaining classifications more confusion was observed in comparison to the map obtained by 10 bands classification. Thus, the most accurate classification (classification based on 10 bands acquired with CASI) was selected and *Z. noltii* classes were merged. Considering the combined class of *Z. noltii*, the producer accuracy increased up to 90.3%, being the user accuracy 97.9%.

The final map (Fig. 5), based on 10 bands acquired with CASI, highly discriminated all estuarine habitat classes. Saltmarshes, vegetated mudflats and green macroalgae presented higher discrimination accuracy than 95%. Whereas, *Phragmites australis* and *Gracilaria* sp. with *Ulva* sp. classes were slightly misclassified, being the producer accuracy of 89% and 81%, respectively.

This map was subsequently compared to the recent GPS-based cartography of the same year undertaken by Garmendia et al. (2013). Focusing in *Z. noltii* meadows, the classification results were consistent (i.e. correct shape of detected areas) with the GPS-based cartography (Fig. 6, dark green areas). However, only 35.2% of the GPS-mapped meadows were correctly classified using CASI imagery. This underestimation was likely produced due to the large extents of seagrass meadows which are low dense within the intertidal areas of the estuary and CASI cannot detect them (Fig. 6a, light green areas). In estuarine habitats, in addition to the density related classification issues, factors such as tides also affect remote sensing results. This is the case of the area of Arketas (Fig. 6b) where the largest meadow was not detected, since it was submerged during the image acquisition.

When comparing the *Z. noltii* classified polygons obtained by the CASI classification to the GPS-based cartography, 47.7% of classified polygons were detected to be *Z. noltii* meadows according to the GPS-based cartography. This indicates that there was an overestimation of *Z. noltii* classification, which was located mainly along saltmarsh channels (Fig. 6, red areas). The common *Z. noltii* area between the GPS-based cartography and CASI classification was 25%.

4. Discussion

4.1. Capability of CASI sensor to map estuarine habitats

The accuracy assessment carried out in the present research suggests that mapping has been benefited from the advantages of hyperspectral data since accurate distribution has been achieved for almost all the habitat classes. The highest and most consistent mean accuracy values were recorded for the 10 band combination (MPA 91.8% and MUA 93.7%). These results were corroborated by the kappa coefficient of agreement (0.98). The classification using almost the full set of configured CASI bands (i.e. including all the spectral bands except for bands 1 and 2) was not found to be the most accurate classification. Overall accuracy measurements were not as consistent as in the classification based on the 10 bands combination. The low accuracy values obtained for the combination of the three visible bands conventionally used for photo-interpretation, indicates that hyperspectral data are more adequate for image classification than aerial visible photography. Chust et al. (2008) also found high percentage of classification error when only conventional visible bands were used in the classification. Our results support the commonly reported importance of infrared wavelengths for estuarine species classification (Costa et al., 2007; Chust et al., 2008, 2010; Phinn et al., 2008). Thus, despite the high cost of the hyperspectral data acquisition and the complex data processing, CASI imagery provides a wider range of information (i.e. several habitats) and it can cover large and inaccessible areas, allowing the acquisition of comparable time-series information.

4.2. Classification of Z. noltii meadows

Z. noltii class distribution was found to be accurate based on the validation results but when comparing to the GPS-based cartography from Garmendia et al. (2013) a low agreement was found mainly because low dense and submerged areas of *Z. noltii* were not detected by CASI. The main reason of these contrasting results is

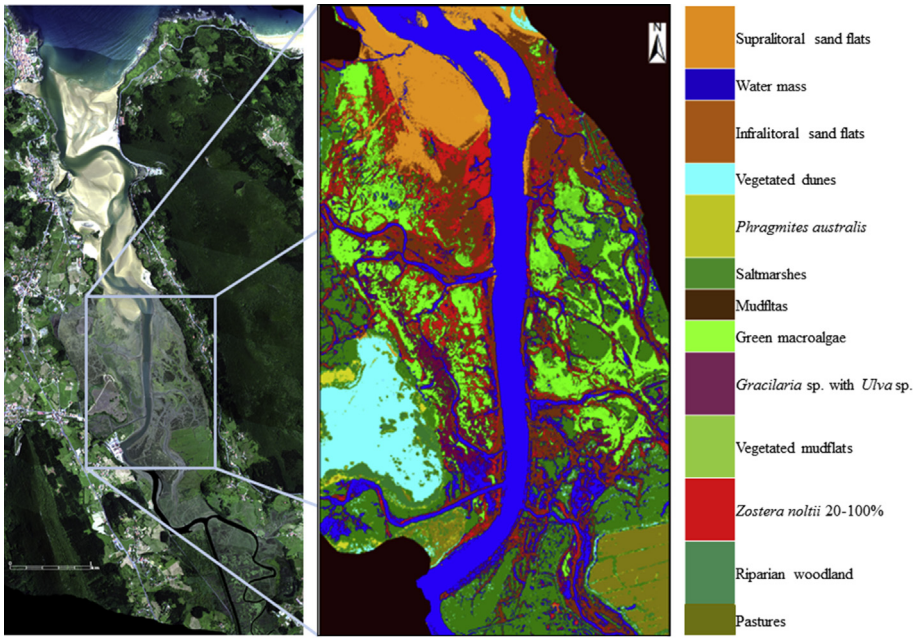

Fig. 5. a) Oka estuary (RGB: bands 23, 16, 6) and classified image based on 10 bands; b) zoom to San Cristobal and Kanala intertidal areas.

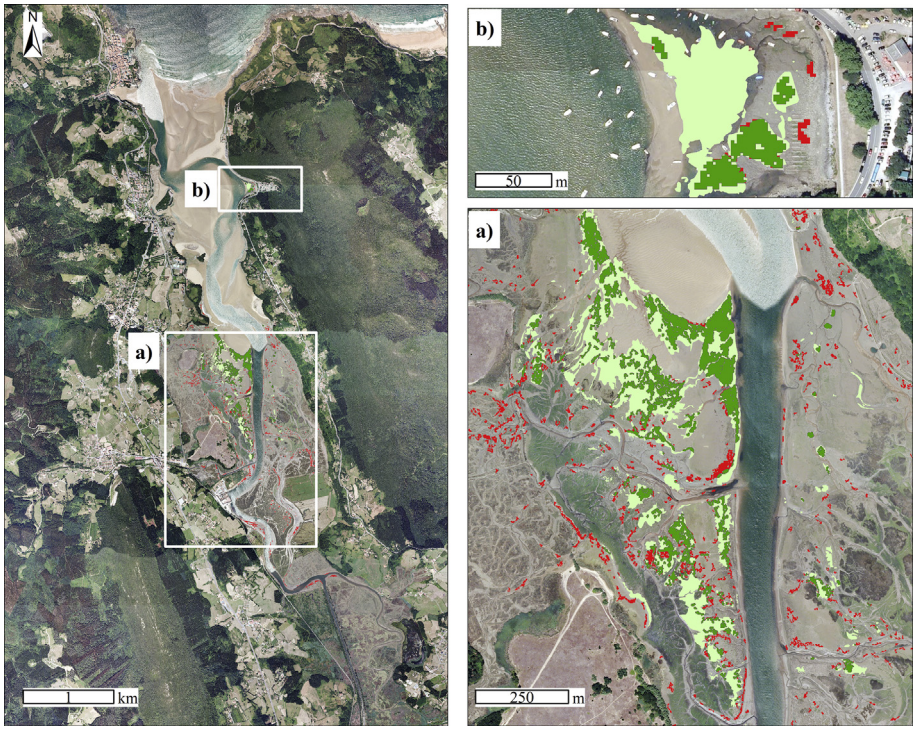

Fig. 6. *Zostera noltii* distribution corresponding to the combination of the GPS-based cartography from Garmendia et al. (2013) and the classification based on 10 bands of the Compact Airborne Spectrographic Imager (CASI). a) San Cristobal and Kanala intertidal areas; b) Arketas zone. In dark green, agreement areas (i.e. shared polygons GPS and CASI); in light green, areas mapped only by GPS-based cartography (i.e. polygons mapped using GPS but not detected by CASI classification); in red, areas only classified by CASI classification (i.e. polygons produced by CASI classification where there is not *Z. noltii* according to GPS-based cartography). (For interpretation of the references to colour in this figure legend, the reader is referred to the web version of this article.)

that overall accuracy values were based on the validation sites which were undertaken within homogeneous patches of *Z. noltii* not affected by the edge. Hence, the classification results must be considered with caution, suggesting that reliable mapping of *Z. noltii* using CASI sensor must be restricted to moderate and high dense meadows. Krause-Jensen et al. (2004) already indicated that meadows of low density may not always be detected and the sensitivity of the mapping is therefore higher for dense meadows than for sparsely vegetated meadows. The GPS-based cartography of *Z. noltii* meadows carried out by Garmendia et al. (2013) at the same period, allowed us to assess this sensitivity and to detect the constraints of the CASI method when classifying seagrass beds. The

GPS-based cartography of *Z. noltii* meadows undertaken by Garmendia et al. (2013), although requiring longer sampling time, was less expensive, more reliable and the data processing was faster. However, this method is only appropriate for small and accessible estuaries and for a low number of target species. On the contrary, as mentioned above, despite the higher cost of the hyperspectral data acquisition and the more complex data processing, CASI imagery provides a wider range of information (i.e. several habitats) and it can cover large and inaccessible areas, allowing the acquisition of comparable time-series information. Thus, rather than replacement, the integration of both techniques should be considered in order to complement estuarine habitat monitoring (Lyons et al., 2013).

4.3. Normalized difference vegetation index for Z. noltii

In the present research we have defined an $NDVI_z$ which was applied to determine a percent cover threshold in the basis of which two habitat classes of the species were determined. Similar NDVIs have been applied to detect changes in the distribution of *Z. noltii* seagrass (Barillé et al., 2010; Bargain et al., 2013) suggesting that the acquired CASI imagery could be used to develop further research on the applicability of the index for mapping the percentage of species cover. As pointed by Bargain et al. (2012), vegetation indices for seagrass mapping must be applied with caution, due to their high sensibility to the background influences of sediment. That influence has been recorded in this research since some ROIs with lower percent cover of *Z. noltii* presented high $NDVI_z$ values.

The specific sampling of *Z. noltii* meadows allowed to assess the changes on the spectral response of the species at different percent covers. The obtained results were in accordance with Bargain et al. (2012) where an orderly decrease of reflectance in the visible part of the spectrum, with deeper absorption at 675 nm and a shaper increase in the near-infrared plateau was observed with a biomass increase. As pointed out by Dekker et al. (2006), a spectral library collection of estuarine habitats should be very useful supporting the field of hyperspectral remote sensing in coastal habitats.

4.4. Concluding remarks and perspectives

1 Airborne hyperspectral imagery is useful for mapping estuarine habitats, although accurate *Z. noltii* classification has been found to be restricted to moderate and high dense meadows. In this sense, of note is the importance of elevation and topographical features in habitat classification pointed out by Chust et al. (2010). Considering that the *Z. noltii* niche is strongly associated with a narrow range of terrain elevation and the high dependence of the estuarine habitats to the terrain elevation, the integration of digital terrain models with the hyperspectral imagery would probably enhance the map classification accuracy. Therefore, the simultaneous acquisition from two airborne sensors (CASI and LiDAR) might strongly improve habitat cartography and environmental monitoring as suggested by Collin et al. (2010).

2 The vegetation index NDVIz is capable of discriminating between sparsely vegetated and dense *Z. noltii* beds and thus, can be further applied to CASI imagery in order to map the percentage of species cover in those areas where the species is present.

3 Airborne hypespectral data provide relevant information for biodiversity monitoring at spatial and temporal scales. Derived information on habitat distribution could also be coupled with environmental data in order to model the suitable habitat of each habitat class and future projections under climate change scenarios could be undertaken (Valle et al., 2014). Thus, obtained data could provide key information to be used in supporting the implementation of environmental legislation, protection and conservation of coastal habitats, and to establish adaptation plans to face climate change impacts.

Acknowledgements

This investigation was funded by the Basque Water Agency (URA) under an agreement with AZTI; likewise by the Ministry of Economy and Competitiveness of the Spanish Government (Project Ref.: CTM2011-29473). M. Valle has benefited from a PhD Scholarship granted by the Iñaki Goenaga - Technology Centres Foundation. We wish to thank the botanist Amador Prieto for his support in plant species identification which was essential for a correct classification of the different habitats analysed, Mercedes Herrera from the Flora and Vegetation Research Group of the University of the Basque Country (UPV/EHU) for her valuable comments on (Table 2) and Iñigo Onandia from AZTI for the photographs taken during the field sampling carried out. Finally, the authors greatly acknowledge the CNES for funding the SYNIHAL project. The comments from the editor and three anonymous reviewers have improved considerably the first manuscript draft. This paper is contribution number 728 from AZTI (Marine Research Division).

Appendix A. Supplementary data

Supplementary data related to this article can be found at http://dx.doi.org/10.1016/j.ecss.2015.07.034.

References

Alamús, R., Talaya, J., Colomina, I., 1999. The SISA/0: ICC Experiences in Airborne Sensor Integration. Joint Workshop of ISPRS WG I/1. In: I/3 and IV/4: Sensors and Mapping from Space (Hannover, Germany).

Babey, S.K., Soffe, R.J., 1992. Radiometric calibration of the airborne spectrographic imager (CASI). Can. J. Remote Sens. 18, 233–242.

Barbier, E.B., Hacker, S.D., Kennedy, C., Koch, E.W., Stier, A.C., Silliman, B.R., 2011. Estuarine and coastal ecosystems and their services. Ecol. Monogr. 81, 169–193.

Bargain, A., Robin, M., Le Men, E., Huete, A., Barillé, L., 2012. Spectral response of the seagrass *Zostera noltii* with different sediment backgrounds. Aquat. Bot. 98, 45–56.

Bargain, A., Robin, M., Méléder, V., Rosa, P., Le Menn, E., Harin, N., Barillé, L., 2013. Seasonal spectral variation of *Zostera noltii* and its influence on pigment-based vegetation Indices. J. Exp. Mar. Biol. Ecol. 446, 86–94.

Barillé, L., Robin, M., Harin, N., Bargain, A., Launeau, P., 2010. Increase in seagrass distribution at Bourgneuf Bay (France) detected by spatial remote sensing. Aquat. Bot. 92, 185–194.

Beaumont, N., Austen, M., Atkins, J.P., Burdon, D., Degraer, S., Dentinho, T., Derous, S., Holm, P., Horton, T., van Ierland, E., Marboe, A., Starkey, D., Townsend, M., Zarzycki, T., 2007. Identification, definition and quantification of goods and services provided by marine biodiversity: implications for the ecosystem approach. Mar. Pollut. Bull. 54, 253–265.

BOPV, 2011. Orden de Modificación del Catálogo Vasco de Especies Amenazadas de la Fauna y Flora Silvestre y Marina, 2011 February 23 BOPV-Basque Country Oficial Bull. 37 (937), 12.

Borja, Á., Aguirrezabalaga, F., Martínez, J., Sola, J.C., García-Arberas, L., Gorostiaga, J.M., 2004. Benthic communities, biogeography and resources management. In: Borja, Á., Collins, M. (Eds.), Oceanography and Marine Environment of the Basque Country. Elsevier Oceanography Series, Amsterdam, pp. 455–492.

Borja, Á., Galparsoro, I., Solaun, O., Muxika, I., Tello, E.M., Uriarte, A., Valencia, V., 2006. The European water framework directive and the DPSIR, a methodological approach to assess the risk of failing to achieve good ecological status. Estuar. Coast. Shelf Sci. 66, 84–96.

Castro, R., Uriarte, A., Martínez de Murguía, A., Borja, Á., 2004. Biodiversity and conservation of wildlife and natural habitats. In: Borja, Á., Collins, M. (Eds.), Oceanography and Marine Environment of the Basque Country. Elsevier Oceanography Series, Amsterdam, pp. 537–574.

Chen, J.M., Leblanc, S.G., Miller, J.R., Freemantle, J., Loechel, S.E., Walthall, C.L., Innanen, K.A., White, H.P., 1999. Compact airborne spectrographic imager (CASI) used for mapping biophysical parameters of boreal forests. J. Geophys. Res. 104, 27945–27958.

Chust, G., Galparsoro, I., Borja, Á., Franco, J., Uriarte, A., 2008. Coastal and estuarine habitat mapping, using LIDAR height and intensity and multi-spectral imagery.

Estuarine. Coast. Shelf Sci. 78, 633–643.
Chust, G., Grande, M., Galparsoro, I., Uriarte, A., Borja, Á., 2010. Capabilities of the bathymetric Hawk Eye LiDAR for coastal habitat mapping: a case study within a Basque estuary. Estuar. Coast. Shelf Sci. 89, 200–213.
Collin, A., Long, B., Archambault, P., 2010. Salt-marsh characterization, zonation assessment and mapping through a dual-wavelength LiDAR. Remote Sens. Environ. 114, 520–530.
Colomina, I., Alamús, R., Palà, V., Castillo, M., 1995. First experiences with the CASI scanner at the ICC. In: 3rd International Workshop High Precision Navigation, Stuttgart, Germany.
Congalton, R.G., 1991. A review of assessing the accuracy of classifications of remotely sensed data. Remote Sens. Environ. 37, 35–46.
Costa, M., Loos, E.A., Shaw, A., Steckler, C., Hill, P., 2007. Hyperspectral imagery for mapping intertidal vegetation at Roberts Bank tidal flats, British Columbia, Canada. Can. J. Remote Sens. 33, 130–141.
Costanza, R., D'Arge, R., de Groot, R.S., Farber, S., Grasso, M., Hannon, B., Naeem, S., Limburg, K., Paruelo, J., O'Neill, R.V., Raskin, R., Sutton, P., van den Belt, M., 1997. The value of the world's ecosystem services and natural capital. Nature 387, 253–260.
Costanza, R., de Groot, R.S., Sutton, P., van der Ploeg, S., Anderson, S.J., Kubiszewski, I., Farber, S., Turner, R.K., 2014. Changes in the global value of ecosystem services. Glob. Environ. Change 26, 152–158.
Dehouck, A., Lafon, V., Lubac, B., Kervella, S., Bru, D., Schmeltz, M., Roubache, A., 2012. Hyperspectral field database in support to coastal wetland mapping. In: IGARSS, pp. 2649–2652.
Dekker, A.G., Brando, V.E., Anstee, J.M., 2005. Retrospective seagrass change detection in a shallow coastal tidal Australian lake. Remote Sens. Environ. 97, 415–433.
Dekker, A.G., Brando, V.E., Anstee, J.M., Fyfe, S.K., Malthus, T., Karpouzli, E., 2006. Remote sensing of seagrass systems: use of spaceborne and airborne systems. In: Larkum, A.W.D., Orth, R., Duarte, C.M. (Eds.), Seagrasses: Biology, Ecology and Conservation. Springer, Dordrecht, The Netherlands, pp. 347–359.
Duarte, C.M., 2002. The future of seagrass meadows. Environ. Conserv. 29, 192–206.
Finkbeiner, M., Stevenson, B., Reaman, R., 2001. Guidance for Benthic Habitat Mapping: an Aerial Photographic Approach. NOAA Coastal Services Center, Charleston, SC, USA, p. 79.
Foody, G.M., 2002. Status of land cover classification accuracy assessment. Remote Sens. Environ. 80, 185–201.
Fyfe, S.K., 2003. Spatial and temporal variation in spectral reflectance: are seagrass species spectrally distinct. Limnol. Oceanogr. 48, 464–479.
Garmendia, J.M., Valle, M., Borja, Á., Chust, G., Franco, J., 2013. Cartografía de *Zostera noltii* en la costa vasca: cambios recientes en su distribución (2008-2012). Rev. Investig. Mar. 20, 1–22.
Green, E.P., Short, F.T., 2003. World Atlas of Seagrasses. Prepared by the UNEP World Conservation Monitoring Centre. University of California Press, Berkeley. USA, p. 298.
Halpern, B.S., Walbridge, S., Selkoe, K.A.K., Kappel, C.V., Micheli, F., D'Agrosa, C., Bruno, J.F., Casey, K.S., Ebert, C., Fox, H.E., Fujita, R., Heinemann, D., Lenihan, H.S., Madin, E.M.P., Perry, M.T., Selig, E.R., Spalding, M., Steneck, R., Watson, R., Heineamann, D., 2008. A global map of human impact on Marine ecosystems. Science 319, 948–952.
Herkül, K., Kotta, J., Kutser, T., Vahtmäe, E., 2013. Relating remotely sensed optical variability to marine benthic biodiversity. PLoS One 8, e55624.
Hoepffner, N., 2006. Marine and Coastal Dimension of Climate Change in Europe. A report to the European Water Directors. Institute for Environmental Sustainability, Joint Research Center, European Communities, p. 107.
IPCC, 2014. Summary for policymakers. In: Field, C.B., Barros, V.R., Dokken, D.J., Mach, K.J., Mastrandrea, M.D., Bilir, T.E., Chatterjee, M., Ebi, K.L., Estrada, Y.O., Genova, R.C., Girma, B., Kissel, E.S., Levy, A.N., MacCracken, S., Mastrandrea, P.R., White, L.L. (Eds.), Climate Change 2014: Impacts, Adaptation, and Vulnerability. Part a: Global and Sectoral Aspects, Contribution of Working Group II to the Fifth Assessment Report of the Intergovernmental Panel on Climate Change. Cambridge University Press, Cambridge, United Kingdom and New York, NY, USA, pp. 1–32.
Jensen, J.R., 2007. Remote Sensing of the Environment: an Earth Resource Perspective, second ed. Prentice-Hall, Upper Saddle River, p. 592.
Jollineau, M.Y., Howarth, P.J., 2008. Mapping an inland wetland complex using hyperspectral imagery. Int. J. Remote Sens. 29, 3609–3631.
Krause-Jensen, D., Quaresma, A.L., Cunha, A.H., Greve, T.M., 2004. How is seagrass habitat quality monitored? In: Borum, J., Duarte, C.M., Krause-Jensen, D., Greve, T.M. (Eds.), European Seagrasses: an Introduction to Monitoring and Management. EU Project Monitoring and Managing of European Seagrasses, Copenhagen, Denmark, pp. 45–53.
Light, D.L., 1986. Satellite photogrammetry. Manual of photogrammetry. In: Slama, C.C. (Ed.), American Society of Photogrammetry, Falls Church, Virginia, pp. 883–977.
Lillesand, M.T., Kiefer, R., 2000. Remote Sensing and Image Interpretation, fourth ed. John Wiley and Sons, New York, p. 736.
Lotze, H.K., 2010. Historical reconstruction of human-induced changes in U.S. estuaries. Oceanogr. Mar. Biol. Annu. Rev. 48, 267–338.
Lyons, M.B., Roelfsema, C.M., Phinn, S., 2013. Towards understanding temporal and spatial dynamics of seagrass landscapes using time-series remote sensing. Estuar. Coast. Shelf Sci. 120, 42–53.
Martínez, L., Palà, V., Arbiol, R., Pérez, F., Tardà, A., 2006. Atmospheric Correction Algorithm Applied to CASI Multi-height Hyperspectral Imagery. In: Quantitative Remote Sensing. Torrent, Valencia, Spain.
Mumby, P.J., Green, E.P., Edwards, A.J., Clark, C.D., 1997. Measurement of seagrass standing crop using satellite and digital airborne remote sensing. Mar. Ecol. Prog. Ser. 159, 51–60.
Peneva, E., Griffith, J.A., Carter, G.A., 2008. Seagrass mapping in the northern Gulf of Mexico using airborne hyperspectral imagery: a comparison of classification methods. J. Coast. Res. 244, 850–856.
Phinn, S., Roelfsema, C.M., Dekker, A.G., Brando, V.E., Anstee, J.M., 2008. Mapping seagrass species, cover and biomass in shallow waters: an assessment of satellite multi-spectral and airborne hyper-spectral imaging systems in Moreton Bay (Australia). Remote Sens. Environ. 112, 3413–3425.
Rönnbäck, P., Kautsky, N., Pihl, L., Troell, M., Söderqvist, T., Wennhage, H., 2007. Ecosystem goods and services from Swedish coastal habitats: identification, valuation, and implications of ecosystem shifts. Ambio 36, 534–544.
Rouse, J.W.J., Haas, R.H., Schell, J.A., Deering, D.W., 1973. Monitoring vegetation systems in the Great Plains with ERTS. In: Third ERTS Symposium, NASA SP-351. U.S. Gov. Printing Office, pp. 309–317.
Stehman, S.V., 1997. Selecting and interpreting measures of thematic classification accuracy. Remote Sens. Environ. 62, 77–89.
Thorhaug, A., Richardson, A.D., Berlyn, G.P., 2007. Spectral reflectance of the seagrasses: *Thalassia testudinum, Halodule wrightii, Syringodium filiforme* and five marine algae. Int. J. Remote Sens. 28, 1487–1501.
Tucker, C.J., 1979. Red and photographic infrared linear combinations for monitoring vegetation. Remote Sens. Environ. 8, 127–150.
Valle, M., Borja, Á., Chust, G., Galparsoro, I., Garmendia, J.M., 2011. Modelling suitable estuarine habitats for *Zostera noltii*, using ecological niche factor analysis and bathymetric LiDAR. Estuarine Coast. Shelf Sci. 94, 144–154.
Valle, M., Chust, G., del Campo, A., Wisz, M.S., Olsen, S.M., Garmendia, J.M., Borja, Á., 2014. Projecting future distribution of the seagrass *Zostera noltii* under global warming and sea level rise. Biol. Conserv. 170, 74–85.
Waycott, M., Duarte, C.M., Carruthers, T.J.B., Orth, R.J., Dennison, W.C., Olyarnik, S., Calladine, A., Fourqurean, J.W., Heck, K.L., Hughes, R.G., Kendrick, G.A., Kenworthy, W.J., Short, F.T., Williams, S.L., 2009. Accelerating loss of seagrasses across the globe threatens coastal ecosystems. Proc. Natl. Acad. Sci. 106, 12377–12381.
Wong, P.P., Losada, I.J., Gattusso, J.P., Hinkel, J., Khattabi, A., McInnes, K., Saito, Y., Sallenger, A., 2014. Coastal systems and low-lying areas. In: Field, C.B., Barros, V.R., Dokken, D.J., Mach, K.J., Mastrandrea, M.D., Bilir, T.E., Chatterjee, M., Ebi, K.L., Estrada, Y.O., Genova, R.C., Girma, B., Kissel, E.S., Levy, A.N., MacCracken, S., Mastrandrea, P.R., White, L.L. (Eds.), Climate Change 2014: Impacts, Adaptation, and Vulnerability. Part a: Global and Sectoral Aspects, Contribution of Working Group II to the Fifth Assessment Report of the Intergovernmental Panel on Climate Change. Cambridge University Press, Cambridge, United Kingdom and New York, NY, USA.
Worm, B., Barbier, E.B., Beaumont, N., Duffy, J.E., Folke, C., Halpern, B.S., Jackson, J.B.C., Lotze, H.K., Micheli, F., Palumbi, S.R., Sala, E., Selkoe, K.A., Stachowicz, J.J., Watson, R., 2006. Impacts of biodiversity loss on ocean ecosystem services. Science 314, 787–790.